

# X-ray observation of AM Herculis in a very low state with *Suzaku*

Y. Terada<sup>1</sup>, M. Ishida<sup>2,3</sup>, A. Bamba<sup>2,4</sup>, K. Mukai<sup>5</sup>, T. Hayashi<sup>2,3</sup>, and A. Harayama<sup>1</sup>  
 terada@phy.saitama-u.ac.jp

## ABSTRACT

The X-ray observation of AM Her in a very low state was performed with *Suzaku* in October 2008. One flare event with a time scale of  $\sim 3700$  sec was detected at the X-ray luminosity of  $6.0 \times 10^{29}$  erg sec<sup>-1</sup> in the 0.5 – 10 keV band assuming at a distance of 91 pc. The X-ray spectrum is represented by a thermal plasma emission model with a temperature of  $8.67^{+1.31}_{-1.14}$  keV. During the quiescence out of the flare interval, *Suzaku* also detected significant X-rays at a luminosity of  $1.7 \times 10^{29}$  erg sec<sup>-1</sup> in the 0.5 – 10 keV band, showing a clear spin modulation at a period of 0.1289273(2) days at BJD 2454771.581. The X-ray spectra in the quiescence were represented by a MEKAL + Power Law (PL) model or a single CEMEKL model, which are also supported by phase-resolved analyses. A correlation between the temperature and the volume emission measure was found together with historical X-ray measurements of AM Her in various states. In order to account for a possible non-thermal emission from AM Her, particle acceleration mechanisms in the AM Her system are also discussed, including a new proposal of a shock acceleration process on the top of the accretion column.

*Subject headings:* novae, cataclysmic variables – stars: individual (AM Herculis) – plasmas – acceleration of particles

## 1. Introduction

Since white dwarfs (WDs) exist everywhere in our Galaxy and have so large number density that one third of all the astronomical galactic objects are WDs (Allen 1973), they have some possibilities to make important contributions to unresolved long-standing mysteries in the astrophysics, such as the origin of Cosmic-ray particles, Galactic ridge emissions, and so on. Therefore, it is important to understand the nature of

WDs in detail. Magnetic cataclysmic variables (MCVs) are binary systems which consist of late type stars and WDs with strong magnetic field strength of over  $10^5$  G. Cold gases from a companion star via a Roche-Lobe overflow accrete onto the magnetic pole(s) of the WD, and release their gravitational potentials at the standing shock on the WD surface. The temperature of the shock heated plasma, called an accretion column, reaches about  $10^8$  K, and the plasma emits hard X-rays via bremsstrahlung process (see the review by Patterson 1994). Polars are sub-class of MCVs, which have so strong magnetic field strength of  $> 10^7$  G that spin periods of WDs are synchronized to the orbital periods.

In this paper, we report on the X-ray observation of the proto-type star of polars, AM Her, with *Suzaku* (Mitsuda et al. 2007). The distance to the object  $d$ , the magnetic field strength on the surface of the WD,  $B_{\text{WD}}$ , the mass of the WD,  $M_{\text{WD}}$ , its radius,  $R_{\text{WD}}$ , and the spin period,  $P_{\text{spin}}$ , are measured as  $d = 91$

<sup>1</sup>Department of Physics, Science, Saitama University, 255 Simo-Ohkubo, Sakura-ku, Saitama city, Saitama 338-8570, Japan

<sup>2</sup>Department of High Energy Astrophysics, Institute of Space and Astronautical Science (ISAS), Japan Aerospace Exploration Agency (JAXA), 3-1-1 Yoshinodai, Sagami-hara, Kanagawa 229-8510, Japan

<sup>3</sup>Science of Physics, Tokyo Metropolitan University, 1-1 Minami-Osawa, Hachioji-si, Tokyo, 192-0397, Japan

<sup>4</sup>School of Cosmic Physics, Dublin Institute for Advanced Studies, 31 Fitzwilliam Place, Dublin 2, Ireland

<sup>5</sup>Exploration of the Universe Division, Code 660, NASA/GSFC, Greenbelt, MD 20771, USA

pc (Gänsicke et al. 1995),  $B_{\text{WD}} = 13\text{--}30$  MG (Schmidt et al. 1981, 1983; Wickramasinghe et al. 1984; Wickramasinghe & Martin 1985),  $M_{\text{WD}} = 0.39\text{--}1.2 M_{\odot}$  (Young et al. 1981; Mukai and Charles 1987; Bailey et al. 1988; Cropper et al. 1998), and  $P_{\text{spin}} = 3.09$  hr (Stockman et al. 1977), respectively, where  $M_{\odot}$  and  $R_{\odot}$  are the mass and radius of the Sun, respectively. Due to changes of an accretion rate,  $\dot{M}$ , from the companion star, the optical flux of AM Her shows two states; the high state with V magnitude of 13.5 mag and the low state with 15.5 mag. The previous X-ray observations in high states are performed by *HEAO-1* (Rothschild et al. 1981), *EXOSAT* (Osborne et al. 1986), *Ginga* (Ishida et al. 1991; Beardmore et al. 1995; Cropper et al. 1998), and *ASCA* (Ishida et al. 1997; Terada et al. 2004). They all report the detail measurements of the thermal emission from the accretion column of AM Her. On the other hand, X-ray observations in the low state are reported only by *BeppoSAX* (Matt et al. 2000), and those in an intermediate state are covered by *Chandra* (Girish et al. 2007).

X-ray studies of thermal emissions in a low state can help us to understand the physics of the accretion flow by exploring one of the important physical parameters,  $\dot{M}$ , in a wide range. In addition, in a very low state, it should be easier to search for unknown faint emissions behind the thermal radiation. One of possible new-type components is a non-thermal emission as suggested by Terada et al. (2008b) from *Suzaku* observations of an intermediate polar AE Aqr, which belongs to a sub-class of MCVs having weaker magnetic field strength than polars. Although the observation was actually not in a low state, the high-sensitive wide-band spectroscopy and phase-resolved analyses enabled them to find spiky pulsations like neutron star (NS) pulsars in the spin profiles with two independent instruments on-board *Suzaku*. They claimed that these spikes may have non-thermal origin from detailed analyses of X-ray spectra. Thus, the object is now called as a “NS pulsar equivalent of WD” (de Jager 1994) or just a “WD pulsar”. X-ray deep observations in very low states could provide such a discovery; a second “WD pulsar”, which is important in studies of searches for a new cosmic-ray acceleration system. In this paper, we describe the X-ray observation of AM Her in a low state in section 2, summarize

the results of *Suzaku* analyses during the flare and the quiescence in section 3, and discuss in section 4.

## 2. Observation and Data Reduction

### 2.1. *Suzaku* observation of AM Her

*Suzaku* is the fifth series of the Japanese X-ray satellite, carrying two X-ray instruments; the X-ray Imaging Spectrometer (XIS; Koyama et al. 2007) and the Hard X-ray Detector (HXD; Takahashi et al. 2007). It has good capabilities to provide very low-background observations with high sensitivities in the 0.2 – 600 keV bandpass. Thus, it is suitable to search for a hidden emission from a faint object with a wide-band spectroscopy. In addition, high timing capability with the time resolution of 8 sec and 64  $\mu\text{sec}$  for the XIS and the HXD, respectively (Terada et al. 2008a), can help us to follow the fast variability of the object.

We observed AM Her with *Suzaku* from 2008 October 29 20:22 UT to November 1 07:18 UT on the HXD-nominal position (OBSID=403007010; hereafter AMHER). According to optical reports by the American Association of Variable Star Observers (AAVSO) <sup>1</sup>, this observation date corresponds to the low state of the object lasting from September 2008 to June 2009. In addition to the main observation tagged as AMHER, we also performed an off-axis observation near the object to have the best use of the *Suzaku* sensitivities from 2008 November 1 07:18 UT to November 2 08:15 UT (OBSID = 403008010; hereafter AMHER\_OFF\_AXIS). The off-axis observation was carried out towards the position of (RA, DEC)=(282.08, 47.99), where no hard X-ray sources are contaminated in the field of view of the HXD PIN and GSO. On both occasions, the XIS was operated in the normal clocking mode without window/burst options but with the Space Charge-Injection (SCI) function (Nakajima et al. 2008). The HXD was operated in the nominal mode; half of 64 PIN diodes were operated with a voltage of 400 V and the others with 500 V.

### 2.2. Data Reduction

We used the data sets by the standard *Suzaku* pipe-line processing version 2.2.11.22, with the cal-

<sup>1</sup><http://www.aavso.org>

TABLE 1  
SOURCE LIST IN THE BACKGROUND REGION.

| OBSID     | RA           | DEC          | Flux <sup>†</sup>                      | index <sup>‡</sup>                     | Identification                     |
|-----------|--------------|--------------|--|--|------------------------------------|
| 403007010 | 18:17:10.379 | +49:47:06.95 | 4.80 <sup>+1.16</sup> <sub>-1.13</sub> | 1.33 <sup>+0.34</sup> <sub>-0.31</sub> | 1WGA J1817.1+4947                  |
| 403007010 | 18:16:34.923 | +49:48:32.84 | 1.90 <sup>+0.49</sup> <sub>-0.49</sub> | 2.57 <sup>+0.67</sup> <sub>-0.65</sub> | SUZAKU J1816.6+4948.5 <sup>§</sup> |
| 403008010 | 18:48:04.720 | +47:57:34.24 | 6.73 <sup>+1.13</sup> <sub>-1.13</sub> | 2.07 <sup>+0.31</sup> <sub>-0.32</sub> | SUZAKU J1848.0+4757.6 <sup>§</sup> |
| 403008010 | 18:48:17.747 | +47:52:25.25 | 2.41 <sup>+1.27</sup> <sub>-2.40</sub> | 2.44 <sup>+1.42</sup> <sub>-1.26</sub> | SUZAKU J1848.3+4752.4 <sup>§</sup> |

<sup>†</sup> X-ray flux in 0.5 – 10 keV band,  $10^{-14}$  erg sec<sup>-1</sup> cm<sup>2</sup>.

<sup>‡</sup> Photon index of the object.

<sup>§</sup> Newly discovered with *Suzaku* in this work.

ibration version (CALDBVER) of hxd20081009, xis20081009, xrt20080709, and xrs20060410. We used the ftools in HEADAS 6.6 with XSPEC version 11.3.2ag.

The source was detected with the XIS at the average count rate of 0.03 – 0.04 cnt sec<sup>-1</sup> per sensor in the 0.5 – 10 keV band. Cleaned events of the XIS data were obtained with the standard criteria of the pipe-line process. The exposures of AMHER and AMHER\_OFF\_AXIS observations were 108.5 ksec and 44.3 ksec, respectively. On-source events of the XIS were then obtained by accumulating within 6 mm (4.3 $\prime$ ) radius from the image centroid of the object in the AMHER dataset. Several faint sources (including one known object) were detected both in AMHER and AMHER\_OFF\_AXIS datasets with the XIS count rate of less than about 0.005 cnt sec<sup>-1</sup>, which is comparable to the count rate of the background and corresponds to the X-ray flux of  $0.7 \times 10^{-13}$  erg sec<sup>-1</sup> cm<sup>2</sup> as listed in table 1. Thus, the background events were accumulated by source free regions of AMHER and AMHER\_OFF\_AXIS, where  $> 6$  mm outer than these faint sources or AM Her. We summed up these two background spectra, because these spectral shapes and the flux of the two blank sky datasets were consistent within 5 % in the 0.5 – 10 keV range.

In the data reduction of the HXD, we first reprocessed the unscreened events by the tool 'hxdpi' and 'hxdgrade' (Terada et al. 2005) using the CALDB files (including the GSO gain-history file named ae\_hxd\_gsoght\_20090131.fits to

correct the PMT gains of GSO), and then obtained cleaned events of PIN and GSO with the standard criteria of the process. The exposures of the HXD of AMHER and AMHER\_OFF\_AXIS were 94.4 ksec and 40.3 ksec, respectively. The non X-ray background (NXB) events of PIN and GSO are estimated and provided by the HXD team with the methods by Fukazawa et al. (2009). We used NXB events of both PIN and GSO with METHOD='LCFITDT (bgd\_d)' and version of METHODV='2.0ver0804'. The systematic errors of the NXB can be checked by comparison between the actual data and the NXB data during the night earth observations. In AMHER and AMHER\_OFF\_AXIS observations, from night earth spectra with exposures of 38 ksec and 59 ksec for PIN and GSO, respectively, the reproducibilities of PIN and GSO NXBs were about 4 and 1 %, respectively. Within these systematic errors, the events detected with PIN were consistent with the Cosmic X-ray background (CXB) level, and those with GSO were consistent with being no signals.

### 3. Analyses and Results

#### 3.1. X-ray Light Curves

Fig. 1 shows background-subtracted light curves of AM Her, obtained with the XIS and the HXD. The arrival times in this figure are barycentric corrected with the tool named 'aebarycen' (Terada et al. 2008a). In the XIS data, a flare phenomenon starting from BJD 2454770.78 was observed with a duration of about 7 ksec. There was not any brightening in the background data

of the XIS, and so the flare should arise from AM Her itself. On the other hand, the PIN data showed no significant flare synchronized to the XIS one. Here, we defined the duration between BJD 2454770.777416 – 2454770.863308 as an epoch of the flare, and the others as the quiescence. The effective exposures of the XIS during the flare and the quiescence were 5.0 ksec and 103 ksec, respectively.

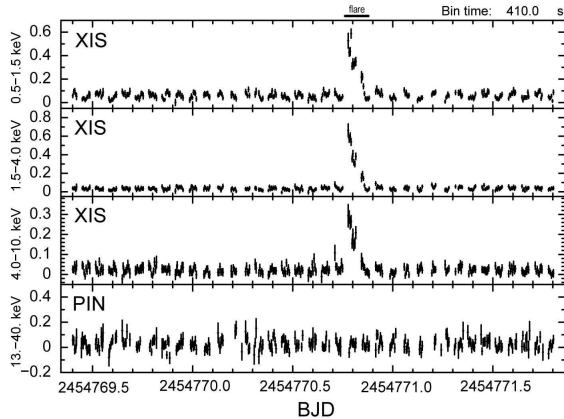


Fig. 1.— Background subtracted light curves taken with the *Suzaku* XIS and HXD in 0.5 – 1.5, 1.5 – 4.0, 4.0 – 10.0, 13 – 40 keV band, from top to bottom, respectively.

We search for the spin period from the XIS data in the 0.5 – 10 keV band during the quiescence, and obtained the period  $P_{\text{XIS}} = 0.1289273(2)$  days at the epoch BJD 2454771.581. The value is consistent with the  $P_{\text{spin}}$  by previous observations (Stockman et al. 1977; Kafka et al. 2005); i.e.,  $P_{\text{XIS}} = P_{\text{spin}}$ . Here, the epoch was simply determined by the peak time of the pulse profile fitted with the sine function. Fig. 2 shows the energy-resolved light curves folded at  $P_{\text{XIS}}$ . Clear spin modulations are observed especially in the soft energy band below 4 keV. They have similar pulse shapes to those taken with *ASCA* (Tanaka et al. 1994) during the high state, although significant energy dependence of the spin amplitudes is detected, unlike those in high states (Ishida et al. 1997).

### 3.2. X-ray Properties during the Flare

Fig. 3 shows the light curve of the XIS in the 0.5 – 10 keV band around the flare. The folded

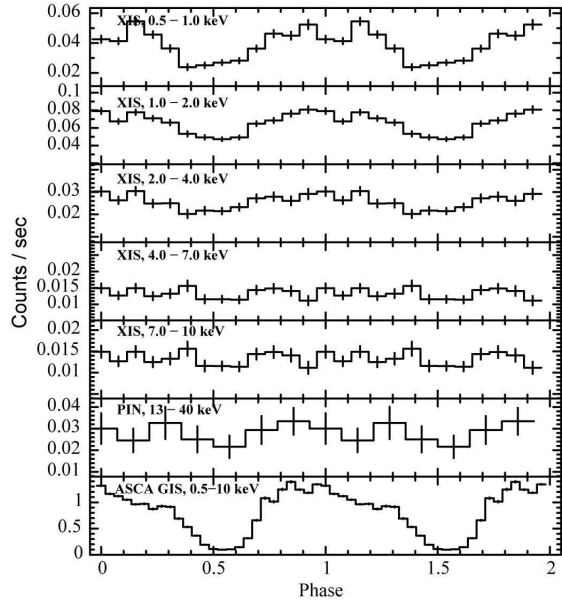


Fig. 2.— Light curves folded at the spin period of  $P_{\text{XIS}} = 0.1289273$  days shown in 0.5 – 1.0, 1.0 – 2.0, 2.0 – 4.0, 4.0 – 7.0, 7.0 – 10.0, and 13 – 40 keV band from the top to bottom panels, respectively. The phase 0.0 corresponds to BJD 2454771.581. The upper six panels are taken with *Suzaku*, and the lowest panel shows the same plot but with *ASCA* GIS in 1993 (Terada et al. 2004).

0.5 - 10 keV light-curve in the quiescence (like Fig. 2) are overlaid periodically for comparison. If we subtract this spin variation, X-ray counts around the phase bottom (BJD 2454770.86 – 2454770.88) became almost zero, but the others showed an exponential decay. Then, we fitted the light curve without the phase-bottom epoch by the exponential function of  $\exp((T - T_0)/\tau_{\text{flare}})$ , where  $T$ ,  $T_0$ , and  $\tau_{\text{flare}}$  are time, starting time of the flare, and a decay constant of time, respectively. We obtained the time origin of  $T_0 = \text{BJD } 2454770.76 \pm 0.03$  and the decay constant of  $\tau_{\text{flare}} = (4.3 \pm 0.2) \times 10^{-2}$  days.

The X-ray spectra during the flare are shown in Fig. 4. Since there were no significant detections by the PIN and GSO within systematic errors of the NXB (section 2.2), only XIS events were plotted in the figure. First, we tried to reproduce the X-ray spectra by an emission model from an optically-thin thermal plasma, which can be generated at the post-shock region

TABLE 2  
BEST FIT MODEL PARAMETERS IN THE FLARE EPOCH OF AM HER.

| Model          | $n_{\text{H}}$<br>$10^{20} \text{ cm}^{-2}$ | $kT$<br>keV            | $\alpha$ ‡             | abundance<br>solar     | Flux†<br>$10^{-12} \text{ erg cm}^{-2} \text{ s}^{-1}$ | $\chi^2_{\nu}$ (d.o.f) |
|----------------|---|------------------------|------------------------|------------------------|--|------------------------|
| phabs * MEKAL  | < 1.3                                       | $8.67^{+1.31}_{-1.14}$ | ...                    | $0.76^{+0.28}_{-0.26}$ | $5.96^{+0.11}_{-0.26}$                                 | 1.00 (205)             |
| phabs * CEMEKL | < 4.0                                       | $17.6^{+13.9}_{-6.6}$  | $1.64^{+0.70}_{-0.65}$ | $0.90^{+0.40}_{-0.35}$ | $6.05^{+0.02}_{-0.38}$                                 | 0.99 (203)             |

† X-ray flux in 0.5 – 10 keV band.

‡ The power of  $DEM$ , as presented by  $DEM \propto (T/T_{\text{max}})^{\alpha-1}d(T)$  in the CEMEKL model (Done & Osborn 1997).

of the accretion gas-flow onto the WD via energy releases of their gravitational potential. The spectra obtained with *Suzaku* were well reproduced by such a thin-thermal plasma model called MEKAL (Mewe et al. 1985; Liedahl et al. 1995; Kaastra et al. 1996), as shown in table 2 and Fig. 4. The fitting to the XIS-0, 1, and 3 datasets were performed simultaneously, and cross normalizations were consistent with the value of 1.0. Although the temperature,  $kT = 8.67^{+1.31}_{-1.14}$  keV, obtained during this very low state, was slightly lower than those in high states (e.g., 13.5 keV or 11 keV by Beardmore et al. 1995; Ishida et al. 1997, respectively) the metal abundance,  $0.76^{+0.28}_{-0.26}$  solars, was consistent with values in high states. Thus, the hot plasma would come from the accretion matters from the companion star. The spectra requires no significant photo-electric absorption as shown in table 2; this fact is also self-consistent with the situation of a very low accretion rate.

You may notice that there remains a line structure around 2.0 keV in the residual plot of Fig. 4, although they were insignificant. If it was real, the features should come from a light element Si, from which emission should be suppressed in such a high temperature as  $kT = 8.67$  keV. For a reference, we further tried an one-dimensional cooling-flow model as originally proposed by Hōshi (1973) and Aizu (1973), and found that no more free parameters improve the fitting statistically. The spectra were also well fitted by such a model as the CEMEKL model (Done & Osborn 1997; Baskill et al. 2005), but there was no large improvement in the chi-squared value, as shown in table 2. In this fitting, the shock temperature,

$T_{\text{max}}$ , were obtained as  $17.6^{+13.9}_{-6.6}$  keV, which is higher than the average temperature by the single MEKAL fitting, because  $T_{\text{max}}$  represents the maximum temperature just below the shock front in the accretion plasma. The value itself was reasonable compared with the gravitational potential of the WD. The power of the temperature gradient,  $\alpha$ , of the differential emission measure,  $DEM$ , was  $\alpha = 1.64^{+0.70}_{-0.65}$ , which was different from the theoretical expectation of 0.5 (Ishida et al. 1994) with a simple assumption of an one-dimensional stable cooling-flow by Aizu (1973)

### 3.3. Average Spectral Analysis in the Quiescence

The X-ray spectra during the quiescence with *Suzaku* were shown in Fig. 5. Cross normalizations between XIS-0, XIS-1, and XIS-3 were consistent with 1.0, as already checked in section 3.2, and thus datasets of all the XIS chips were summed in the figure. As implied in section 3.1 and Fig. 2, the spin pulse profile during the quiescence shows the similar modulations as in the high states, soft X-ray emissions should have thermal origin. Therefore, we tried to represent the spectrum by a single MEKAL model, following the steps on the analyses during the flare (section 3.2), but the fitting was not acceptable ( $\chi^2_{\nu} = 1.30$ ) as shown in table 3. The metal abundance was quite low as  $0.06^{+0.03}_{-0.02}$  solar, and so the best fit model has no physical meanings.

In the hard X-ray band, the spin pulse profiles (Fig. 2) showed shallower modulations than those in the softer energy band; the pulse shape was consistent with being flat in above 10 keV range.

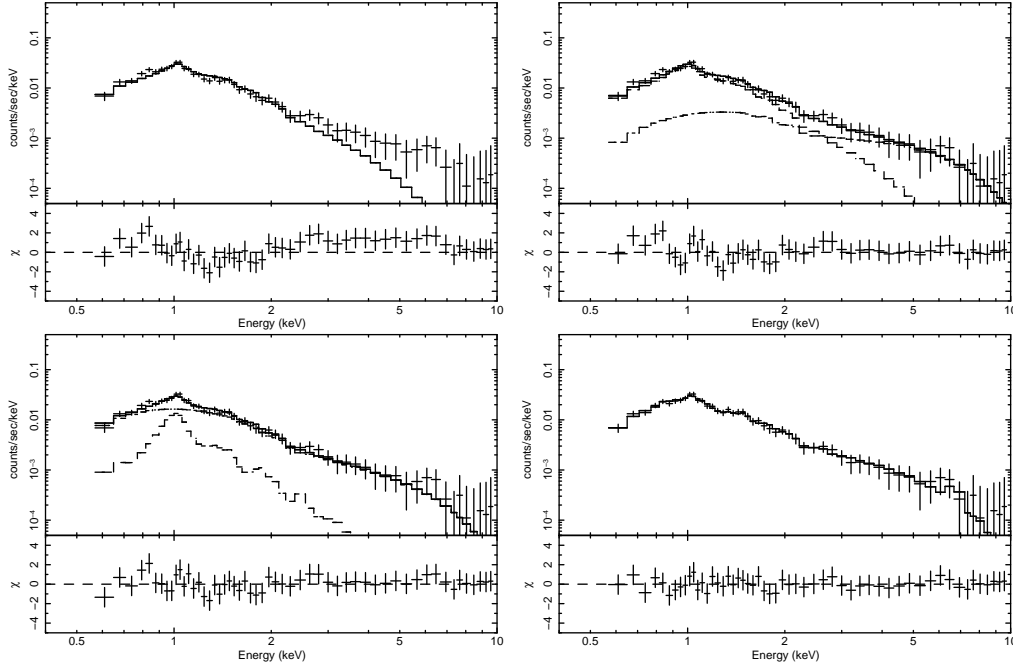


Fig. 5.— X-ray spectra with *Suzaku* during the quiescence of AM Her in the very low state. The crosses represents the XIS data summed of XIS-0, XIS-1, and XIS-3. Lines show the best fit models of single MEKAL, double MEKAL, MEKAL + power law, and CEMEKL, in top left, top right, bottom left and bottom right panels, respectively (see the text). Parameters of the models are listed in table 3.

Thus, in the spectral analyses, we then added another component in the hard X-ray band, representing another thermal emission (case-1) or non-thermal component (case-2).

In the first case that hard X-rays have a thermal origin (case-1), we tried a double MEKAL model to represent the spectrum. As a result, the fitting became acceptable ( $\chi^2_\nu = 0.76$ ), as shown in table 3 and Fig. 5. However the temperature of the higher component was quite high as  $> 17.7$  keV and the metal abundance was still too low as  $0.06^{+0.02}_{-0.02}$  solar, compared with the result during the flare (section 3.2) and/or reports by previous observations in high states (Ishida et al. 1997; Terada et al. 2004; Girish et al. 2007). In the fitting, the two parameters of the abundance in both MEKAL components were linked, but the situation did not change even when we set these two parameters free from each other;  $1.03^{+0.05}_{-0.06}$  keV plasma with abundance of  $0.06^{+0.01}_{-0.01}$  solar and  $> 14.8$  keV plasma with  $< 0.85$  solar abundance ( $\chi^2_\nu = 1.01$ ).

In the second case that hard X-rays have a

non-thermal origin (case-2), we tried MEKAL + PL model and obtained an acceptable result ( $\chi^2_\nu = 0.61$ ), as shown in table 3 and Fig. 5. The metal abundance of the MEKAL component,  $0.80^{+0.40}_{-0.15}$  solar, became consistent with previous observations (Ishida et al. 1997; Terada et al. 2004; Girish et al. 2007) and this work during the flare (section 3.2). The photon index of the non-thermal component was  $2.36^{+0.15}_{-0.14}$ . The X-ray flux in the 0.5 – 10 keV band of the non-thermal component was  $(1.5 \pm 0.1) \times 10^{-13}$  erg sec $^{-1}$  cm $^{-2}$ , which corresponds to the luminosity in the same energy band of  $(1.5 \pm 0.1) \times 10^{29} \left(\frac{d}{91\text{pc}}\right)^2$  erg sec $^{-1}$ . Note that a hump structure around 6 – 7 keV in the residual panel of Fig. 5 bottom left was statistically insignificant; if we tentatively add a Gaussian model here to MEKAL + PL model, we obtained the central energy of the Gaussian at  $6.3^{+2.1}_{-6.3}$  keV, where the improvement of  $\chi^2_\nu$  was only 0.02 corresponding to the F-test value and the probability of 1.76 and 0.18, respectively.

As an application of case-1 fitting (double MEKAL model), we also tried the multi-color

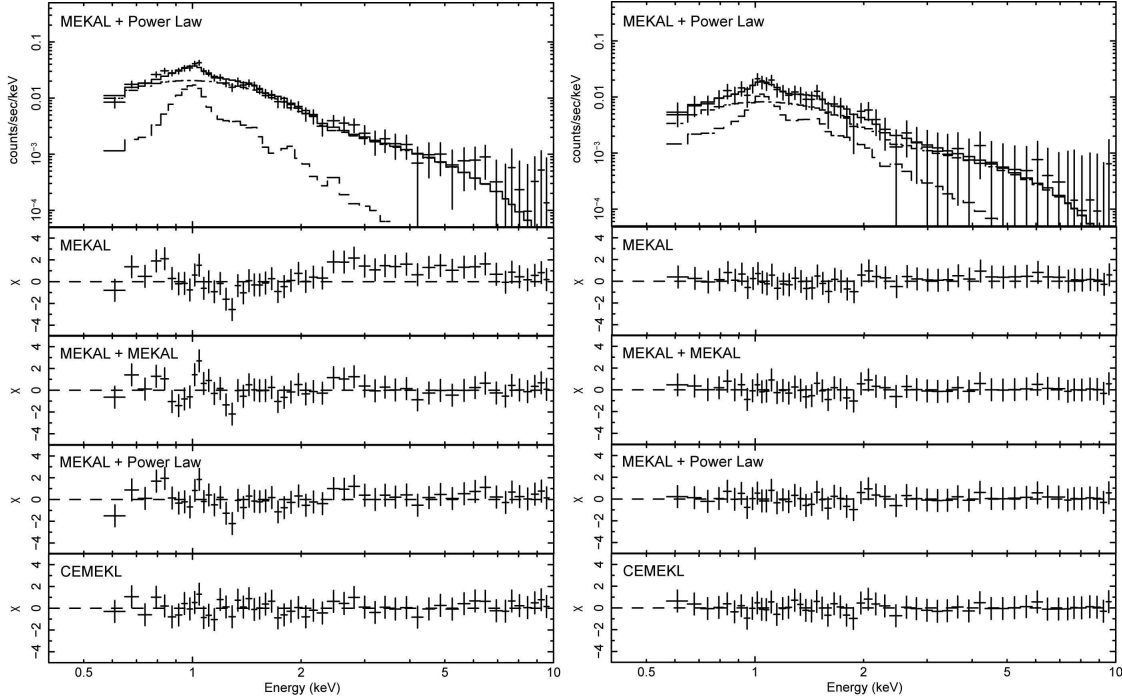


Fig. 6.— Left and right panels show the X-ray spectra in the top and bottom phases, respectively. Crosses are the XIS data. The top panel in each figure shows the spectrum with the best fit model of MEKAL + power law, and bottom panels are the residuals of data from models, MEKAL, MEKAL+MEKAL, MEKAL+Power Law, and CEMEKL, towards lower panels. Parameters of the models are summarized in table 3.

plasma model, CEMEKL, as already used in section 3.2 (case-3), and got an acceptable result ( $\chi^2_\nu = 0.32$ ) as summarized in table 3 and Fig. 5. The metal abundance and the  $kT_{\max}$  of the best fit model were reasonable as  $0.48^{+0.22}_{-0.21}$  solar and  $6.37^{+8.34}_{-1.37}$  keV, respectively. The power  $\alpha$  of the Volume Emission Measure (VEM) was  $\alpha = 0.58^{+0.31}_{-0.18}$ , which was consistent with the theoretical value of  $\alpha = 0.5$  (Ishida et al. 1994) in an ideal situation of the one-dimensional steady cooling flow. In summary, the phase-averaged X-ray spectrum of AM Her in the quiescence were reproduced not by single MEKAL model, but well by three kinds of models; (case-1) MEKAL + MEKAL, (case-2) MEKAL + PL, and (case-3) CEMEKL, although case-1 requires an unrealistically low metal abundance.

### 3.4. Phase resolved analyses in Quiescence

In order to restrict the emission model in the quiescence, by a combination of results of the tim-

ing analyses (section 3.1) and the spectral ones (section 3.3), we compared the best fit models of the phase-resolved spectra with the spin pulse modulation in Fig. 2, quantitatively.

First, we tried phase-resolved spectral analyses. From the spin profile in Fig. 2, we defined the top and bottom phases as epochs at spin phases of  $\phi = 0.59375 - 1.21875$  and  $0.21875 - 0.59375$ , respectively, and selected XIS events in these two phases. The X-ray spectra in both phases are shown in Fig. 6. Following the phase averaged studies in section 3.3, we tried to fit these spectra with (0) MEKAL, (1) MEKAL+MEKAL, (2) MEKAL+PL, and (3) CEMEKL models, and got results shown in table 3 and Fig. 6. As a result, there were no strict differences statistically among these models except for case-0, single MEKAL model, as already shown in the phase averaged analyses. In addition, the X-ray spectra of the pulsation component (i.e., subtraction from the spectra during the top phase of those during the bottom phase) were also well represented both by thermal and non-thermal

TABLE 3  
BEST FIT MODEL PARAMETERS DURING THE QUIESCENCE OF AM HER.

| Model                | $kT_1$<br>keV          | $kT_2$ or $kT_{\max}$<br>keV | $\alpha^\dagger$ or $\Gamma^\ddagger$ | abundance<br>solar     | Flux $^\S$             | $\chi_\nu^2$ (d.o.f) |
|----------------------|------------------------|------------------------------|---------------------------------------|------------------------|------------------------|----------------------|
| <b>Phase Average</b> |                        |                              |                                       |                        |                        |                      |
| MEKAL                | $1.23^{+0.09}_{-0.13}$ | ...                          | ...                                   | $0.06^{+0.03}_{-0.02}$ | $1.13^{+0.08}_{-0.11}$ | 1.30 (51)            |
| MEKAL + MEKAL        | $1.02^{+0.07}_{-0.11}$ | > 11.1                       | ...                                   | $0.06 \pm 0.02$        | $1.79^{+0.21}_{-0.30}$ | 0.76 (49)            |
| MEKAL + PL           | $1.10 \pm 0.09$        | ...                          | $2.36^{+0.15}_{-0.14}$                | $0.80^{+0.40}_{-0.15}$ | $1.73^{+1.27}_{-0.08}$ | 0.61 (49)            |
| CEMEKL               | ...                    | $6.57^{+3.63}_{-2.57}$       | $0.58^{+0.31}_{-0.18}$                | $0.48^{+0.22}_{-0.21}$ | $1.76^{+0.20}_{-0.54}$ | 0.32 (50)            |
| <b>Top Phase</b>     |                        |                              |                                       |                        |                        |                      |
| MEKAL                | $1.07^{+0.06}_{-0.07}$ | ...                          | ...                                   | $0.05 \pm 0.02$        | $1.62^{+0.14}_{-0.13}$ | 1.24 (51)            |
| MEKAL + MEKAL        | $0.84^{+0.14}_{-0.08}$ | > 6.2                        | ...                                   | $0.04 \pm 0.02$        | $2.36^{+0.14}_{-0.48}$ | 0.73 (49)            |
| MEKAL + PL           | $1.04^{+0.07}_{-0.09}$ | ...                          | $2.42^{+0.17}_{-0.18}$                | $0.80^{+0.56}_{-0.52}$ | $2.13^{+1.85}_{-0.08}$ | 0.67 (49)            |
| CEMEKL               | ...                    | $6.37^{+8.34}_{-1.37}$       | $0.53^{+0.19}_{-0.33}$                | $0.50^{+0.37}_{-0.24}$ | $2.17^{+0.23}_{-0.62}$ | 0.37 (50)            |
| <b>Bottom Phase</b>  |                        |                              |                                       |                        |                        |                      |
| MEKAL                | $1.68^{+0.60}_{-0.37}$ | ...                          | ...                                   | $0.14^{+0.26}_{-0.10}$ | $0.97^{+0.86}_{-0.22}$ | 0.24 (51)            |
| MEKAL + MEKAL        | $1.37^{+0.59}_{-0.35}$ | $79.9^{+0.1}_{-79.8}$        | ...                                   | $0.11^{+2.74}_{-0.09}$ | $1.27^{+0.45}_{-0.31}$ | 0.20 (49)            |
| MEKAL + PL           | $1.43^{+3.07}_{-0.36}$ | ...                          | $2.07^{+6.66}_{-1.65}$                | $0.38^{+0.49}_{-0.31}$ | $1.22^{+0.26}_{-0.14}$ | 0.19 (49)            |
| CEMEKL               | ...                    | $5.76^{+13.0}_{-2.38}$       | $1.29^{+0.73}_{-3.50}$                | $0.76^{+3.17}_{-0.67}$ | $1.26^{+1.11}_{-0.56}$ | 0.17 (50)            |

$\dagger$  Valid for CEMEKL model, the power of *DEM*.

$\ddagger$  Valid for Power law model, the photon Index.

$\S$  The X-ray flux in 0.5 – 10 keV band in  $10^{-13}$  erg cm $^{-2}$  s $^{-1}$ .

TABLE 4  
BEST FIT MODEL PARAMETERS OF THE PULSATION SPECTRUM DURING THE QUIESCENCE.

| Model  | $kT$<br>keV            | $\alpha^\dagger$       | $\Gamma^\ddagger$      | abundance<br>solar     | Flux $^\S$             | $\chi_\nu^2$ (d.o.f) |
|--------|------------------------|------------------------|------------------------|------------------------|------------------------|----------------------|
| PL     | ...                    | ...                    | $3.03^{+0.41}_{-0.39}$ | ...                    | $1.00^{+0.21}_{-0.14}$ | 0.47 (52)            |
| MEKAL  | $0.78 \pm 0.17$        | ...                    | ...                    | $0.05^{+0.08}_{-0.03}$ | $0.73^{+0.16}_{-0.23}$ | 0.32 (51)            |
| CEMEKL | $10.8^{+89.2}_{-10.8}$ | $0.12^{+19.9}_{-0.12}$ | ...                    | $0.84^{+9.16}_{-0.64}$ | $1.00^{+5.47}_{-0.78}$ | 0.27 (50)            |

$\dagger$  Power of the *DEM* in the CEMEKL model,  $\alpha$ .

$\ddagger$  Photon Index of the PL model.

$\S$  X-ray flux in the 0.5 – 10 keV band in  $10^{-13}$  erg cm $^{-2}$  s $^{-1}$ .



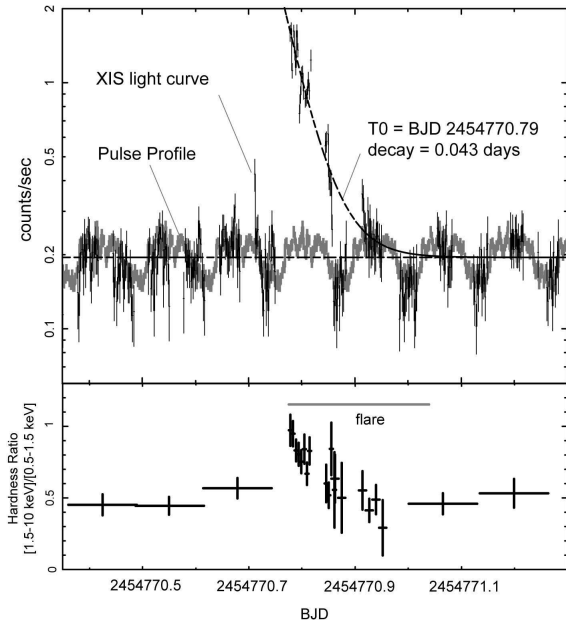


Fig. 3.— Top panel shows the light curves of the XIS in the 0.5 – 10 keV band near the flare event shown in black crosses, and pulse profiles of the XIS in quiescence folded at the spin period of  $P_{\text{XIS}} = 0.1289273$  days are also shown in gray. The dashed lines show the average count of the quiescence and the best-fit exponential curve (see the text). Bottom panel represents the hardness ratio of the XIS; counts in 1.5 – 10.0 keV band divided by those in 0.5 – 1.5 keV band.

models as shown in table 4; i.e., we could not distinguish these origins statistically, only from the phase-resolved analyses.

Next, we evaluated numerically the amplitudes of spin modulations as a function of the energy. Since the modulations are well reproduced by a single sine function (reduced  $\chi^2/\text{d.o.f} \sim 0.6$ ) and power of higher harmonics of the waveform are negligible in estimating amplitudes, we fitted the energy-resolved pulse profiles in Fig. 2 by a sine function with a constant model, and derived the ratios of the pulsation amplitudes to the average ones (i.e., a DC component). As shown in the results in Fig. 7 crosses, it was clearly seen that there were shallower modulations in higher energy band. This situation is different from those seen with *ASCA* in the high state (Ishida et al. 1997). Then, in order to check the consistency of this re-

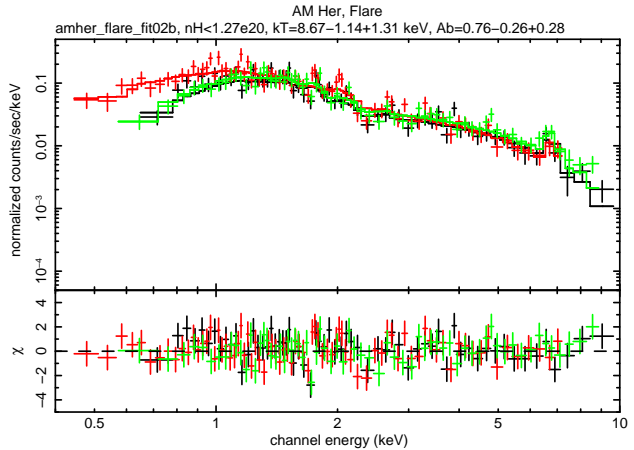


Fig. 4.— X-ray spectra with *Suzaku* during the flare of AM Her in the very low state. The black, red, and green crosses represents the data of XIS-0, XIS-1, and XIS-3, respectively. Lines show the best fit model of MEKAL with parameters in table 2.

sult with phase-resolved spectral models, we also plotted in the same figure the ratios of models between the pulsation components (i.e. subtractions of best fit models in the bottom phase from those in the top) and the best fit models in the average (section 3.3). Therefore, MEKAL + MEKAL model (case-1) requires a large modulation in the hard X-ray band, which was inconsistent with the manner of the spin modulation. The best model was MEKAL + PL (case-2) in Fig. 7, although CEMEKL model (case-3) could not be excluded. Note that the negative values of the ratio seen in the MEKAL+PL model is due to the difference of the best-fit values of the PL index and it is consistent with being 0 above 20 keV.

## 4. Discussions

### 4.1. Plasma Parameters during the Flare

A flare event was observed during the X-ray observation of AM Her in the very low state with *Suzaku*, as shown in section 3.2. Same kinds of flares were reported in other polars, such as UZ For during a low X-ray luminosity Pandel et al. (2002). The X-ray flare of AM Her decayed with a time scale of  $\tau_{\text{flare}} \sim 3700$  sec, and the X-ray spectra was well reproduced by the thermal plasma model with the average temperature of  $kT = 8.7$

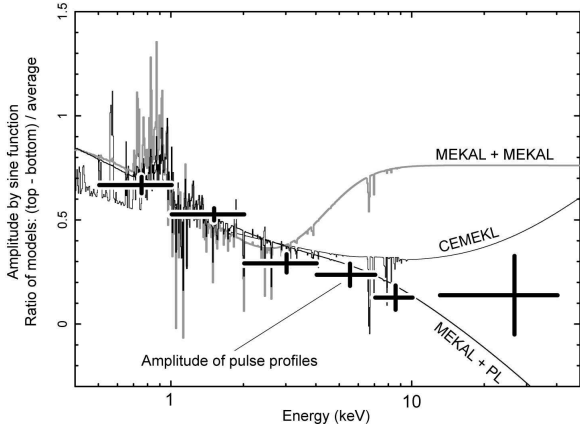


Fig. 7.— Crosses represent the amplitudes of the energy-resolved pulse profiles in Fig. 2 to the average counts (see the text). Lines show the ratio of models taken by phase-resolved spectral analyses in table 3 to the average models; MEKAL + MEKAL, MEKAL + PL, and CEMEKL (Also see the text).

keV (table 2) and the volume emission measure (VEM) of  $3.12 \times 10^{53} \left(\frac{d}{91\text{pc}}\right)^2 \text{cm}^{-3}$ . In this section, we discuss on a rough estimation of plasma parameters during the flare, i.e., the electron density,  $n_e$ , and the plasma size (or the shock height of the plasma,  $h$ ), by using three observational values of  $\tau_{\text{flare}}$ ,  $kT$ , and VEM.

First, from the observational parameter of  $\tau_{\text{flare}}$ , we can estimate the value of  $h$ , if we assume the flare time scale ( $\tau_{\text{flare}}$ ) is mainly determined by the cooling time scale of the plasma,  $\tau_{\text{cool}}$ . This assumption may be correct because the temperature seemed to be gradually decreased through the flare as seen in the bottom panel of Fig. 3. According to Aizu (1973), the shock height is numerically described as  $h = 0.605 \cdot u_s \cdot \tau_{\text{cool}}$ , where  $u_s$  is a shock velocity of the plasma, which is about  $10^9 \text{cm s}^{-1}$  on a typical gravitational potential of a WD in a strong shock case, as

$$u_s = 1.2 \times 10^9 \times \left(\frac{M_{\text{WD}}}{0.88M_{\odot}}\right)^{1/2} \left(\frac{R_{\text{WD}}}{10^9 \text{cm}}\right)^{-1/2} \text{cm s}(\uparrow)$$

Thus, we get

$$h = 3.1 \times 10^{11} \left(\frac{\tau_{\text{cool}}}{3700 \text{s}}\right)$$

$$\times \left(\frac{M_{\text{WD}}}{0.88M_{\odot}}\right)^{1/2} \left(\frac{R_{\text{WD}}}{10^9 \text{cm}}\right)^{-1/2} \text{cm}(2)$$

This value is quite large in the binary system of AM Her compared to the binary distance,  $a$ , which is calculated by the third law of Kepler as

$$a = 9.8 \times 10^{10} \left(\frac{M_{\text{WD}}}{0.88M_{\odot}} + \frac{M_2}{0.3M_{\odot}}\right)^{1/3} \left(\frac{P_{\text{orb}}}{P_{\text{XIS}}}\right)^{2/3} \text{cm}, \quad (3)$$

where  $M_2$  the mass of the companion star (Bailey et al. 1988) and  $P_{\text{orb}}$  is the orbital period of the binary. In other words, this solution requires that the binary space is fully filled with the plasma, and it is unphysical. Therefore, the cooling time scale should be shorter than the flare time scale (i.e.,  $\tau_{\text{cool}} \ll \tau_{\text{flare}}$ ) and  $\tau_{\text{flare}}$  is just described by a time scale of the accretion onto the WD from the companion star. This statement is supported by the observational fact seen in Fig. 3 top; the X-ray flux became faint during the epoch corresponding to the dim phase in quiescence, and thus the flare phenomenon occurs near the magnetic pole on the WD surface.

Second, from the observational parameter of  $kT$ , we can constrain values of  $n_e$  and  $h$ , under the condition that  $\tau_{\text{cool}}$  is not limited by  $\tau_{\text{flare}}$  as discussed above. Here, we use  $n_e$  as the electron density just below the shock front, and we assume that the maximum temperature obtained with the CEMEKL model,  $kT_{\text{max}}$ , represents the shock temperature,  $kT_{\text{sh}}$ , of the multi-color accretion column; i.e., we assume  $kT_{\text{sh}} = kT_{\text{max}}$ . According to Lamb & Masters (1979), the cooling of the plasma occurs via free-free emission and cyclotron radiation, and the time scale of the cooling is described as

$$\tau_{\text{cool}} = \frac{3n_e kT}{2\sqrt{\bar{\epsilon}_{\text{ff}}^2 + \bar{\epsilon}_{\text{cyc}}^2}}, \quad (4)$$

where  $\bar{\epsilon}_{\text{ff}}$  and  $\bar{\epsilon}_{\text{cyc}}$  are the volume-emissivities averaged along the accretion column of the free-free and cyclotron emissions, respectively. The averaged volume-emissivity of free-free emission are quantitatively described as

$$\bar{\epsilon}_{\text{ff}} = A \times 7.3 \times 10^8 \left(\frac{kT_{\text{sh}}}{17.6 \text{keV}}\right)^{1/2} \times \left(\frac{n_e}{5 \times 10^{15} \text{cm}^{-3}}\right)^2 \text{erg sec}^{-1} \text{cm}^{-3}, \quad (5)$$

where  $A$  is a correction factor of the plasma structure; when we put  $z$  as a position from the bottom of the plasma, and the plasma has a vertical dependence of  $kT \propto n_e^{-1} \propto (z/h)^p$ , then  $A$  is described as  $\frac{2}{2-3p}$ . The cyclotron emissivity  $\epsilon_{\text{cyc}}^-$  is given in equation (10) of Wu, Chanmugam, and Shaviv (1994) which depends on  $h^{0.85}$ . Here, the value  $h$  was determined by  $\tau_{\text{cool}}$  in equation (4), which has a dependency with  $\epsilon_{\text{cyc}}^-$  again. Thus, we need to solve the simultaneous equations between  $\bar{\epsilon}_{\text{ff}}$ ,  $\epsilon_{\text{cyc}}^-$ ,  $h$ , and  $n_e$  to get self consistent values. We performed numerical calculations to solve them to derive a rough estimation between  $n_e$  and  $h$ . In the calculation, we assume the Aizu solution (1973) where the cyclotron cooling was ignored; i.e., we assume the relation  $h \sim 0.6u_s\tau_{\text{cool}}$  and set the plasma structure at  $p = 2/5$ . We also ignored the effects of the gradient of the gravitational potential of the WD in the accretion plasma. The solutions, when the magnetic field strength is a typical value of AM Her  $B = 20$  MG (Schmidt et al. 1981), are shown in Fig. 8.

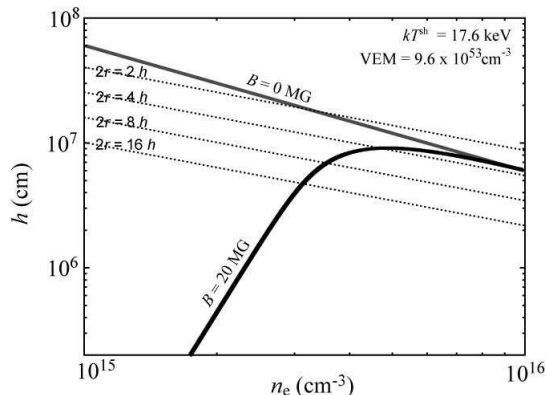


Fig. 8.— Thick lines show numerical solutions of  $h$  and  $n_e$ , based on calculations on  $kT_{\text{sh}}$  with *Suzaku* during the flare phase of AM Her in the very low state. Dashed lines show the limitations from VEM with assumption of  $a = 2, 4, 8, 16$ . See the text.

Finally, we can use the third observational value, VEM, to limit the parameters  $h$  and  $n_e$ . To evaluate the volume of the plasma, we assume that the accretion column has a cylinder shape with a radius of  $r$ , which is  $a$  times size of the shock height (i.e.,  $2r = ah$ ). Dashed lines in Fig.

8 represent the limitation from VEM values to  $h$  and  $n_e$  in cases of  $a = 2, 4, 8$ , and  $16$ . In the plot, we used the VEM value from a simple MEKAL fitting; since the model assumes uniform density and the plot is shown in the shock density, we multiplied a correction factor of  $1/(1-2p)$ , which is 4 when we assume the Aizu solution (1973). As a result, we can get a rough values of  $h$  and  $n_e$  as a function of  $a$ ; for example,  $n_e \sim 5 \times 10^{15} \text{ cm}^{-3}$  and  $h \sim 10^7 \text{ cm}$  when  $a = 4$ . Although many solutions are allowed in this estimation, quite small values of  $a$  are not realistic from Fig. 8; i.e., the plasma has a coin-like shape rather than tall-cylinder one.

#### 4.2. Structure of the Thermal Plasma in the Quiescence

According to the results of the data analyses in sections 3.3 and 3.4, the X-ray spectra of AM Her during the quiescence can be described either by a multi-color-plasma CEMEKL model with a temperature of  $kT_{\text{max}} = 6.7$  keV, or by a combination of thermal and non-thermal model of MEKAL with  $kT = 1.1$  keV plus the PL component. In this section, we focus on the nature of the thermal component, whereas non-thermal phenomena in AM Her will be discussed in the next section 4.3.

First, we estimated the plasma parameters,  $n_e$  and  $h$ , during the quiescence by performing numerical calculations as already shown in section 4.1. The VEMs during the quiescence were one or two order-of-magnitude lower than that in the flare;  $\text{VEM} = 2.5 \times 10^{52} \text{ cm}^3$  (CEMEKL) or  $1.4 \times 10^{51} \text{ cm}^3$  (MEKAL+PL). To obtain the value of  $kT_{\text{sh}}$ , we assumed  $kT_{\text{sh}} = kT_{\text{max}}$  for CEMEKL model as in section 4.1. We cannot estimate  $kT_{\text{sh}}$  directly from  $kT$  of MEKAL model, so we simulated PHA spectra from CEMEKL model with various  $kT_{\text{max}}$  on XSPEC and fitted with MEKAL models to obtain a rough relation between  $kT$  and  $kT_{\text{max}}$ . In the simulation, we used the XIS response on the HXD nominal position and fitted spectra in the hard X-ray band of the XIS, 4 – 10 keV. Then, we got a  $kT_{\text{max}} - kT$  relation as

$$\log(kT_{\text{max}}) \sim 1.23 \log(kT) + 0.14. \quad (6)$$

Thus, the value  $kT = 1.1$  keV by MEKAL analysis corresponds to  $kT_{\text{sh}} \sim 1.6$  keV of the multi-color column. Using these VEM and  $kT_{\text{sh}}$  values, we performed the same numerical calculations again

as in section 4.1, and got plasma parameters as  $n_e \sim$  a few  $\times 10^{14}$   $\text{cm}^{-3}$  and  $h \sim 10^7$  cm when  $a = 4$ . Although there remains an uncertainty on the plasma shape  $a$ , the column height seems to be almost the same order of magnitude as that in flares, and the electron density got one or two order of magnitude lower than in flares.

Second, in order to compare the *Suzaku* results with other past observations in the high, medium, and low states, we plotted  $kT$  and VEM values by several X-ray satellites (Beardmore et al. 1995; Ishida et al. 1997; Matt et al. 2000; Terada et al. 2004; Girish et al. 2007) in Fig. 9. In this figure, the  $kT$  values obtained with MEKAL models are corrected into  $kT_{\text{sh}}$  equivalents by the  $kT$ - $kT_{\text{max}}$  relation of equation (6). Therefore, observationally, the plasma temperature gets lower as VEM gets smaller, and the *Suzaku* points in the faintest state also follow this trend. Hereafter, we call this relation as the VEM -  $kT$  trend.

Finally, to interpret the VEM -  $kT$  trend in Fig. 9 quantitatively, we performed further numerical calculations demonstrated in section 4.1. In Fig. 9, we plotted contours of VEM and  $kT$  with various conditions of  $a$ ,  $n_e$ , and  $h$ . The calculations includes the free-free and cyclotron cooling processes with several assumptions described in section 4.1. Therefore, the results of calculations suggest that the changes on the plasma parameters occur only on  $n_e$ , keeping the column shape almost constant, even when the VEM varies by two order of magnitudes. As shown in Fig. 9, one realistic set of parameters is  $a = 4$  and  $h = 10^7$  cm, which were already presented as an one possible solution of the flare plasma in section 4.1. Other possibilities are larger  $a$  at lower  $h = 10^6$  cm or smaller  $a$  at higher  $h = 10^8$  cm, but the latter case is less feasible because analytic solutions vanish at small  $a$  values, as already mentioned in section 4.1. In other words, our calculation does not exclude other interpretations that both  $n_e$  and the plasma shapes varies as VEM changes.

If the plasma shape is constant in various states keeping the same shock height  $h$ , then the gravitational potentials at the shock front are not changed by its accretion rate. The variation of  $kT$  as observed in Fig. 9 may be caused by possible changes of the energy-conversion efficiency  $\eta$  at the shock, however, the adiabatic index of the accretion gas is required to be less than 1 to change  $\eta$  by

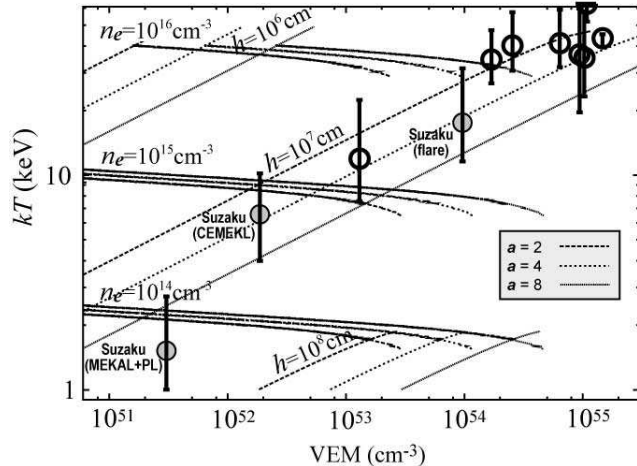


Fig. 9.— Crosses with circle show scatter plot of  $kT$  and VEM, obtained by X-ray observations of AM Her Beardmore et al. (1995); Ishida et al. (1997); Matt et al. (2000); Terada et al. (2004); Girish et al. (2007). Lines show relations between  $kT$  and VEM by numerical calculations on the various cases of  $h = 10^6, 10^7, 10^8$  cm,  $n_e = 10^{14}, 10^{15}, 10^{16}$   $\text{cm}^{-3}$ , and  $a = 2, 4, 8$ . Conditions are shown in the figure.

factor two or three; this situation is not realistic. Another possibility is an observational effect; X-ray observations detect the free-free emissions and thus are essentially sensitive to the dense bottom-part of the column where the plasma is already cooled down mainly by the cyclotron radiation. At lower accretion rate, the effect will be significant because the cyclotron cooling becomes dominant in the lower densities as discussed in section 4.1.

### 4.3. Particle Acceleration on the Accretion Shocks

In this section, we assume that the hard X-ray emission detected with *Suzaku* has non-thermal origin and we concentrate on the particle acceleration processes in AM Her. As demonstrated in sections 3.3 and 3.4, the X-ray luminosity of the power-law component of AM Her was  $L_{\text{x,PL}} = 1.5 \times 10^{29}$  erg  $\text{sec}^{-1}$  at  $d = 91$  pc in 0.5 - 10 keV band, which is the same order of magnitude as that of the first WD-pulsar candidate, AE Aqr, at  $6.6 \times 10^{29}$  erg  $\text{sec}^{-1}$  at  $d = 102$  pc (Terada et al. 2008b). Thus, neither bremsstrahlung nor curva-

ture radiations are feasible as a physical process of non-thermal emissions from a viewpoint of radiation efficiencies, although another possibility is the synchrotron radiation from about MeV electrons under the strong magnetic field of the WD (Terada et al. 2008b).

If particles are accelerated by an electric potential induced by the spin rotation of the magnetized WD up to  $10^{14}$  volts, the acceleration process should occur on the same place as the non-thermal emissions; i.e., near the WD surface where the magnetic field is strong enough to create hard X-rays via synchrotron process. However, in such a polar-cap case, the emissions should present spin pulsations like AE Aqr case, whereas no modulations were observed in the hard X-ray band from AM Her (section 3.1). Thus, electric acceleration mechanism may be less feasible, although we need more theoretical studies. In this section, we further consider another possibility of diffusive shock-acceleration mechanism (Bell 1978; Blandford and Ostriker 1978) on the accretion shock on the pole.

Diffusive shock acceleration mechanism occurs on the collisionless-shock case, which will be realized when the kinetic energy of the plasma particles exceeds the Coulomb potential of the plasma. The ratio between them are called as the binding parameter,  $\zeta$ , and the collisionless shock occurs on the condition of  $\zeta < 1$ . The parameter can be described by

$$\zeta \sim 0.18 \left( \frac{n_e}{10^{15} \text{cm}^{-3}} \right)^{1/3} \left( \frac{kT_{\text{pre}}}{1 \text{eV}} \right)^{-1}, \quad (7)$$

where  $kT_{\text{pre}}$  is a temperature of the pre-shock matters. Therefore, the accretion shock on the WD pole has a condition of a collisionless shock. In the post-shock plasma, according to equation (5.31) by Spitzer (1962) the collisional timescale between the electrons and ions,  $\tau_{\text{ie}}$ , is given as

$$\tau_{\text{ie}} \sim 0.01 \left( \frac{kT_{\text{sh}}}{17.6 \text{keV}} \right)^{3/2} \left( \frac{n_e}{5 \times 10^{15} \text{cm}^{-3}} \right)^{-1} \text{ s}, \quad (8)$$

which is one order of magnitude smaller than the cooling time scale (typically  $\sim 0.3$  sec) by equation (4). Therefore, the collisionless region exists at the top of the accretion column, just beneath the shock, although electrons themselves or protons themselves may be in the collisional equilibrium

under high densities. This idea is supported by the fact that the shallower spin modulation was observed in the harder energy band (section 3.1).

We can assume that the magnetic field is parallel to the shock normal. In this case, the acceleration time-scale on the shock ( $t_{\text{acc}}$ ) is derived as

$$t_{\text{acc}} = \frac{20}{3} \xi \frac{E}{eBu_s^2} c, \quad (9)$$

where  $\xi$ ,  $E$ ,  $e$ ,  $B$  are fluctuation of the magnetic field ( $> 1$ ), the maximum energy of accelerated electrons, electric charge, and the magnetic field strength, respectively (Jokipii 1987; Bamba et al. 2003; Yamazaki et al. 2006). Assuming  $\xi = 1$  (Bohm limit),  $B = 20$  MG, and  $u_s$  at equation (1), the  $t_{\text{acc}}$  becomes

$$t_{\text{acc}} = 2.3 \times 10^{-5} \left( \frac{\xi}{1} \right) \left( \frac{E}{1 \text{TeV}} \right) \left( \frac{B}{20 \text{MG}} \right)^{-1} \times \left( \frac{u_s}{1.2 \times 10^9 \text{cm s}^{-1}} \right)^{-2} \text{ s}, \quad (10)$$

which is very small compared with acceleration time scale in young supernova remnants (e.g., Bamba et al. 2005). In the actual case of the accretion flow onto the WD, the magnetic fluctuation may be  $\xi \gg 1$ , but if it satisfies  $\xi < 10^4$ , the time scale of the acceleration  $t_{\text{acc}}$  is much shorter than the time scale of the accretion  $t_{\text{cool}} \sim 0.3$  s.

The synchrotron loss time scale ( $t_{\text{sync}}$ ) is, on the other hand,

$$t_{\text{sync}} = 9.8 \times 10^{-13} \left( \frac{E}{1 \text{TeV}} \right)^{-1} \left( \frac{B}{20 \text{MG}} \right)^{-2} \text{ s}, \quad (11)$$

from Rybicki & Lightman (1979). The maximum energy of accelerated electron is achieved when the acceleration time-scale becomes same to the synchrotron loss time-scale. The maximum energy of the accelerated electrons is, thus,

$$\left( \frac{E}{1 \text{TeV}} \right) = 2.1 \times 10^{-4} \left( \frac{\xi}{1} \right)^{-1/2} \left( \frac{B}{20 \text{MG}} \right)^{-1/2} \times \left( \frac{u_s}{1.2 \times 10^9 \text{cm s}^{-1}} \right). \quad (12)$$

Our result imply that the accretion shock of CVs can accelerate electrons up to  $\sim \text{GeV}$  when  $\xi = 1$ , which is seen in the cases of young supernova remnants and pulsar wind nebulae. In cases of

$\xi \gg 1$ , which work out when the shock is close to the WD surface and the magnetic field dominates the dynamics of the flow, the maximum energy will be reduced as the dependency of  $\xi^{-0.5}$ ; i.e.,  $E$  will be  $\sim$ MeV at  $\xi = 1000$ . Note that the maximum energy of protons can be  $\sim 1800$  times larger than electrons,  $\sim$  GeV to TeV. The cut-off frequency of synchrotron X-rays ( $\nu_{cut}$ ) is

$$\begin{aligned} \nu_{cut} &= 1.0 \times 10^{18} \left( \frac{E}{1 \text{ TeV}} \right)^2 \left( \frac{B}{20 \text{ MG}} \right) \left( \frac{\xi}{1} \right)^{-1} \text{ Hz} \\ &= 27 \text{ keV} , \end{aligned} \quad (13)$$

which is higher than our observation band, under an assumption of the Bohm limit condition.

## 5. Conclusion

We have observed the polar, AM Her, in a very low state with *Suzaku* at the X-ray luminosity of  $1.7 \times 10^{29} \left( \frac{d}{91 \text{ pc}} \right)^2 \text{ erg sec}^{-1}$  in the 0.5 – 10 keV band.

1. The object shows a flare phenomenon reaching the X-ray luminosity of  $6.0 \times 10^{29} \left( \frac{d}{91 \text{ pc}} \right)^2 \text{ erg sec}^{-1}$  in the 0.5 – 10 keV band, with a time scale of  $\sim 3700 \text{ sec}$  (section 3.1). The X-ray spectra can be reproduced by the thermal-plasma MEKAL model with the temperature of  $8.67_{-1.14}^{+1.31} \text{ keV}$  and the abundance of  $0.76_{-0.26}^{+0.28}$  solars (section 3.2). In discussion on the time scale of the flare, we concluded that it should not be the cooling time scale of the plasma from constraints on the plasma size and density (section 4.1).
2. The X-ray light curves during the quiescence show a clear spin modulation at 0.1289273(2) days at BJD 2454771.581. These values are consistent with those in a high state (section 3.1). The spectra during the quiescence are well represented by MEKAL + PL model or a single CEMEKL model (section 3.3). The phase-resolved analyses also support these two models (section 3.4).
3. From historical X-ray measurements of AM Her in various states, we found that the temperature is positively correlated with the volume emission measure. The *Suzaku* results

in a very low state also follow this relation. We made a rough estimation with a simple numerical calculation, and found that the  $kT$ -VEM trend can be interpreted by a trajectory with a constant plasma shape in various electron densities, as an one of possible solutions (section 4.2).

4. The origin of the non-thermal emission was discussed, and a shock acceleration process at the shock front on the top of the accretion column was checked and proposed (section 4.3).

## Acknowledgement

The authors would like to thank all the members of the *Suzaku* team for their contributions in the maintenance of instruments and software, spacecraft operation, and calibrations. We thank Dr. R. Yamazaki from Aoyama Gakuin University for his useful comments and discussions on the particle acceleration. We also thank Prof. K. Makishima from University of Tokyo and RIKEN for his continuous helps and discussions. We would like to thank the referees and the editor for their careful readings and helpful comments in preparing the paper. This work was supported in part by the Grant-in-Aid for Young Scientists (B) of the MEXT, No. 19740168 (Y. T), and by Grant-in-Aid for Scientific Research of the Japanese Ministry of Education, Culture, Sports, Science and Technology, No. 22684012 (A. B.).

## REFERENCES

- Allen, C. W., 1973, University of London, Athlone Press, 1973, 3rd ed.
- Aizu, K, 1973, Progress of Theoretical Physics, 50, 344
- Abada-Simon, M., Latchkey, A., Bastian, T. S., Bookbinder, J. A., & Dulk, G. A. 1993, ApJ, 406, 692
- Bamba, A., Yamazaki, R., Ueno, M., & Koyama, K. 2003, ApJ, 589, 827
- Bamba, A., Yamazaki, R., Yoshida, T., Terasawa, T., & Koyama, K. 2005, ApJ, 621, 793
- Baskill, Darren S.; Wheatley, Peter J.; Osborne, Julian P. 2005, MNRAS, 357, 626

- Bastian, T. S., Dulk, G. A., & Chanmugam, G. 1988, *ApJ*, 330, 518
- Bailey, J. and Hough, J. H. and Wickramasinghe, D. T., 1988, *MNRAS*, 233, 395
- Beasley, A. J., Bastian, T. S., Ball, L., & Wu, K. 1994, *AJ*, 108, 2207
- Beardmore, A. P., Done, C., Osborne, J. P., Ishida, M., 1995, *MNRAS*, 272, 749
- Bhat, C. L., Kaul, R. K., Rawat, H. S., Senecha, V. K., Rannot, R. C., Sapru, M. L., Tickoo, A. K., & Razdan, H. 1991, *ApJ*, 369, 475
- Bell, A. R., 1978, *MNRAS*, 182, 443
- Blandford, R. D. and Stroker, J. P., 1978, *ApJ*, 221, 29
- Bond, H. E., White, R. L., Becker, R. H., & O'Brien, M. S. 2002, *PASP*, 114, 1359
- Chanmugam, G. & Dulk, G. A. 1982, *ApJ*, 255, L107
- Cropper, Mark, Harrop-Allin, M. K., Mason, K. O., Mittaz, J. P. D., Potter, S. B., Ramsay, Gavin, 1998, *MNRAS*, 293, 57
- de Jager, O. C. 1994, *ApJS*, 90, 775
- de Martino D., Gänsicke, B. T., Matt, G., Mouchet, M., Belloni, T., Beuermann, K., Bonnet-Bidaud, J.-M., Mattei, J., Chiappetti, L., and Done, C. 1998, *Å*, 333, L31
- Done, C., & Osborne, J. P., 1997, *MNRAS*, 288, 649
- Dulk, G. A., Bastian, T. S., & Chanmugam, G. 1983, *ApJ*, 273, 249
- Fukazawa, Y., Mizuno, Y., Watanabe, S., et al. 2009, *PASJ*, 61, S17
- Gänsicke B. T., Beuermann, K., & de Martino, D., 1995, *A&A*, 303, 127
- Girish, V., Rana, V. R., Singh, K. P., 2007, *ApJ*, 658, 525
- Hōshi, R., 1973, *Progress of Theoretical Physics*, 49, 776
- Ishida, M., Silber, A., Bradt, H. V., Remillard, R. A., Makishima, K., Ohashi, T., 1991, *ApJ*, 367, 270
- Ishida, M., Makishima, K., Mukai, K., and Masai, K., 1994, *MNRAS*, 266, 3671
- Ishida, M., Matsuzaki, K., Fujimoto, R., Mukai, K., Osborne, J. P., 1997, *MNRAS*, 287, 651
- Ishida, M., Okada, S., Hayashi, T., Nakamura, R., Terada, Y., Mukai, K., Hamaguchi, K., 2009, *PASJ*, 61, S77
- Jokipii, J.R. 1987, *ApJ*, 313, 842
- Kaastra, J. S., Mewe, R., Nieuwenhuijzen, H. 1996, the 11th Colloquium on UV and X-ray Spectroscopy of Astrophysical and Laboratory Plasmas ,411
- Kafka S., Honeycutt, R., K., Howell, S., B., Harrison, T., E., 2005, *ApJ*, 130, 2852
- Kawka, A., Vennes, S., Schmidt, G. D., Wickramasinghe, D. T., Koch, R., 2007, *ApJ*, 654, 499
- Koyama, K. et al. 2007, *PASJ*, 59, S23
- Nakajima, H., Yamaguchi, H., Matsumoto, H., et al. 2008, *PASJ*, 60, S1
- Lamb, D. Q., & Masters, A. R., 1979, *ApJ*, 234, 117
- Liedahl, Duane A., Osterheld, Albert L., Goldstein, William H., 1995, *ApJ*, 438, 115
- Matt, G., de Martino, D., Gänsicke, B. T., Negueruela, I., Silvotti, R., Bonnet-Bidaud, J. M., Mouchet, M., Mukai, K., 2000, *A&A*, 358, 177
- Mason, P. A. & Gray, C. L. 2007, *ApJ*, 660, 662
- Mewe, R., Gronenschild, E. H. B. M., van den Oord, G. H. J., 1985, *A&AS*, 62, 197
- Meintjes, P. J., de Jager, O. C., Raubenheimer, B. C., Nel, H. I., North, A. R., Buckley, D. A. H., & Koen, C. 1994, *ApJ*, 434, 292
- Meintjes, P. J., Raubenheimer, B. C., de Jager, O. C., Brink, C., Nel, H. I., North, A. R., van Urk, G., & Visser, B. 1992, *ApJ*, 401, 325
- Mitsuda, K et al., 2007, *PASJ*, 59, S1

- Mukai, K., and Charles, P. A., 1987, MNRAS, 226, 209
- Nelson, R. F. & Spencer, R. E. 1988, MNRAS, 234, 1105
- Osborne, J. P., Bonnet-Bidaud, J.-M., Bowyer, S., Charles, P. A., Chiappetti, L., Clarke, J. T., Henry, J. P., Hill, G. J., Kahn, S., Maraschi, L., Mukai, K., Treves, A., Vrtilik, S. 1986, MNRAS, 221, 823
- Pandel, Dirk, Córdova, France A. 2002, MNRAS, 336, 1049
- Patterson J., 1994, PASP, 106, 209
- Pavelin, P. E., Spencer, R. E., & Davis, R. J. 1994, MNRAS, 269, 779
- Rybicki, G. B., & Lightman, A. P. 1979, Radiative Processes in Astrophysics (New York: Wiley Interscience)
- Rothschild, R. E., Gruber, D. E., Knight, F. K., Matteson, J. L., Nolan, P. L., Swank, J. H., Holt, S. S., Serlemitsos, P. J., Mason, K. O., Tuohy, I. R., 1981, ApJ, 250, 723
- Schmidt, G. D., Stockman, H. S., & Margon, B., 1981, ApJ 243, 157
- Schmidt, G. D., Stockman, H. S., Grandi, S. A., 1983, ApJ, 271, 735
- Schmidt, Gary D., Harris, Hugh C., Liebert, James, et al, 2003, ApJ, 595, 1101
- Spitzer, L., 1962, Physics of Fully Ionized Gases, New York Interscience (2nd edition)
- Stockman, H. S., Schmidt, G. D., Angel, J. R. P., Liebert, J., Tapia, S., Beaver, E. A., 1977, ApJ, 217, 815
- Tanaka, Y., Inoue, H., Holt, S. S., 1994, PASJ, 46, L37
- Takahashi, T., et al. 2007, PASJ, 59, S35
- Terada, Y., Kaneda, H., Makishima, K., Ishida, M., et al, 1999, PASJ, 51, 39
- Terada, Y., Ishida, M., Makishima, K., Imanari, T., Fujimoto, R., Matsuzaki, K., Kaneda, H., 2001, MNRAS, 328, 112
- Terada, Y., Ishida, M., Makishima, K., 2004, PASJ, 56, 533
- Terada, Y., Watanabe, S., Ohno, M., Suzuki, M., Itoh, T., Takahashi, I., Sato, G., Murashima, M., Kawano, N., Uchiyama, Y., Kubo, S., Takahashi, T., Tashiro, M., Kokubun, M., Makishima, K., Kamae, T., Murakami, T., Nomachi, M., Fukazawa, Y., Yamaoka, K., Nakazawa, K., and Yonetoku, D., 2005, IEEE TNS 52, 902-909
- Terada, Y., Enoto, T., Miyawaki, R., et al. 2008 PASJ, 60, S25
- Terada, Y., Hayashi, T., Ishida, M., Mukai, K., Dotani, T., Okada, S., Nakamura, R., Naik, S., Bamba, A., Makishima, K., 2008 PASJ 60 387
- Yamazaki, R., Kohri, K., Bamba, A., Yoshida, T., Tsuribe, T., & Takahara, F. 2006, MNRAS, 371, 1975
- Young, P., Schneider, D. P., Sheckman, S. A., 1981, ApJ, 245, 1043
- Wickramasinghe, D. T. & Martin, B., 1985, MNRAS, 212, 353
- Wickramasinghe, D. T., Visvanathan, N., & Tuohy, I. R., 1984, ApJ, 286, 328
- Wu K., Chanmugam, G., Shaviv, G., 1994, Ap&SS, 322, 71